Electronic Supplementary Information

All-organic dielectric polymer films exhibiting superior electric breakdown strength and discharged energy density by adjusting electrode-dielectric interface with organic nano-interlayer

Jia-Yao Pei [a], Shao-Long Zhong [a], Yu Zhao [b, *], Li-Juan Yin [a], Qi-Kun Feng [a], Lei Huang [a], Di-Fan Liu [a], Yong-Xin Zhang [a], Zhi-Min Dang [a, *]

[a] State Key Laboratory of Power System, Department of Electrical Engineering, Tsinghua University, Beijing 100084, China
[b] School of Electrical Engineering, Zheng Zhou University, Henan 450001, China
E-mail: dangzm@tsinghua.edu.cn (Z. M. Dang)
E-mail: zhaoyu19@zzu.edu.cn (Y. Zhao)

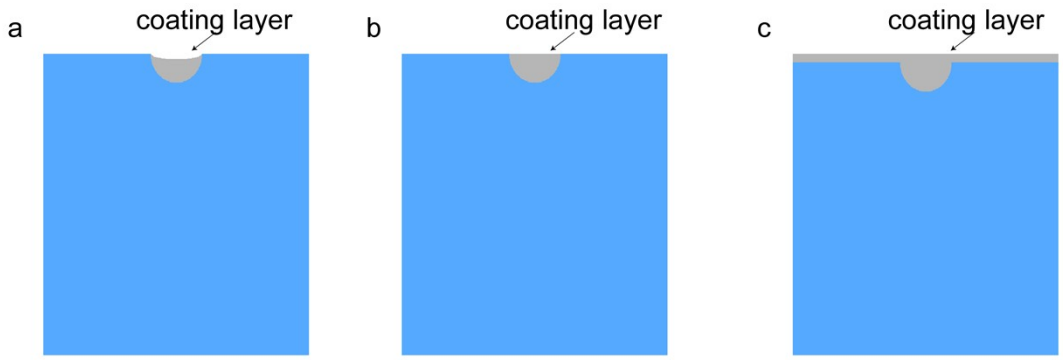

Fig. S1. Schematic drawing of the double-layer structure: (a) under-coating representing the 0.5 wt% PMMA coating films; (b) just-coating representing the 1 wt% PMMA coating films; (c) over-coating representing the 3 wt% PMMA coating films.

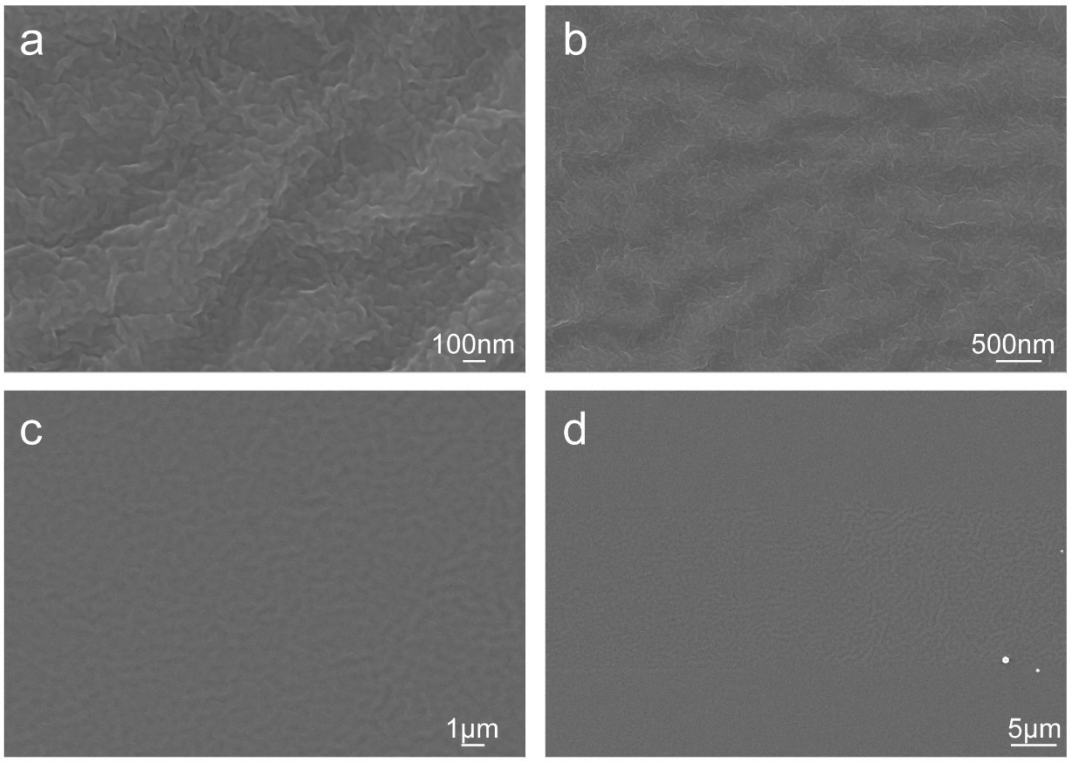

Fig. S2. The smooth side of PVDF films at different magnifications. The ripples in the picture come from the electron bombardment during the SEM test, not from the sample itself

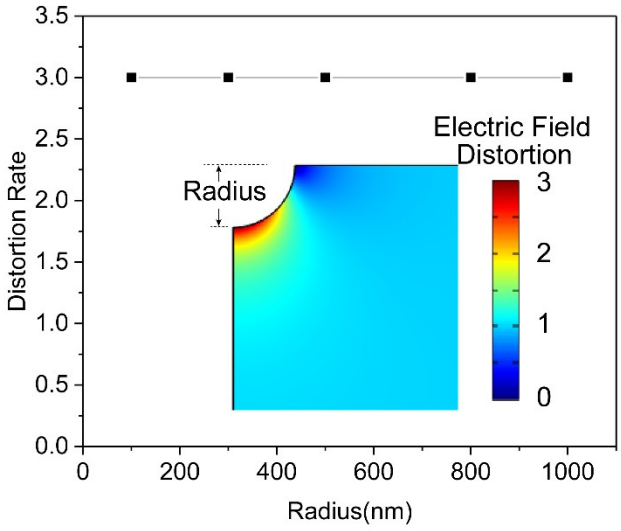

Fig. S3. Variation of distortion rate with the variation of hole radius. The insets illustrate the electric field distortion near the electrode-dielectric interface.

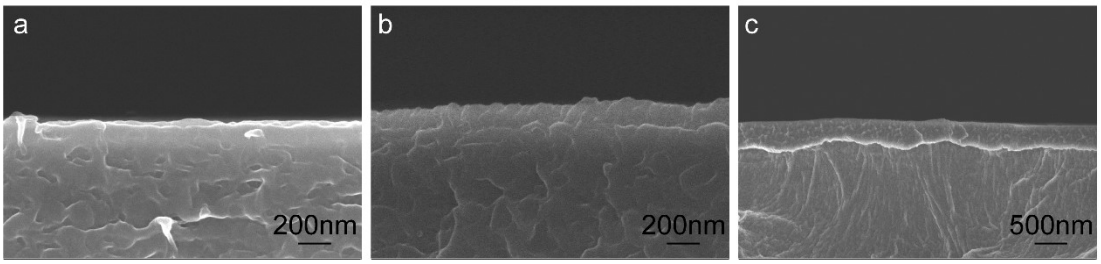

Fig. S4. Cross-sectional SEM images of polymer films with different spinning coating solution with mass fraction (**a**)0.5wt%, (**b**) 1wt%, (**c**) 3wt%.

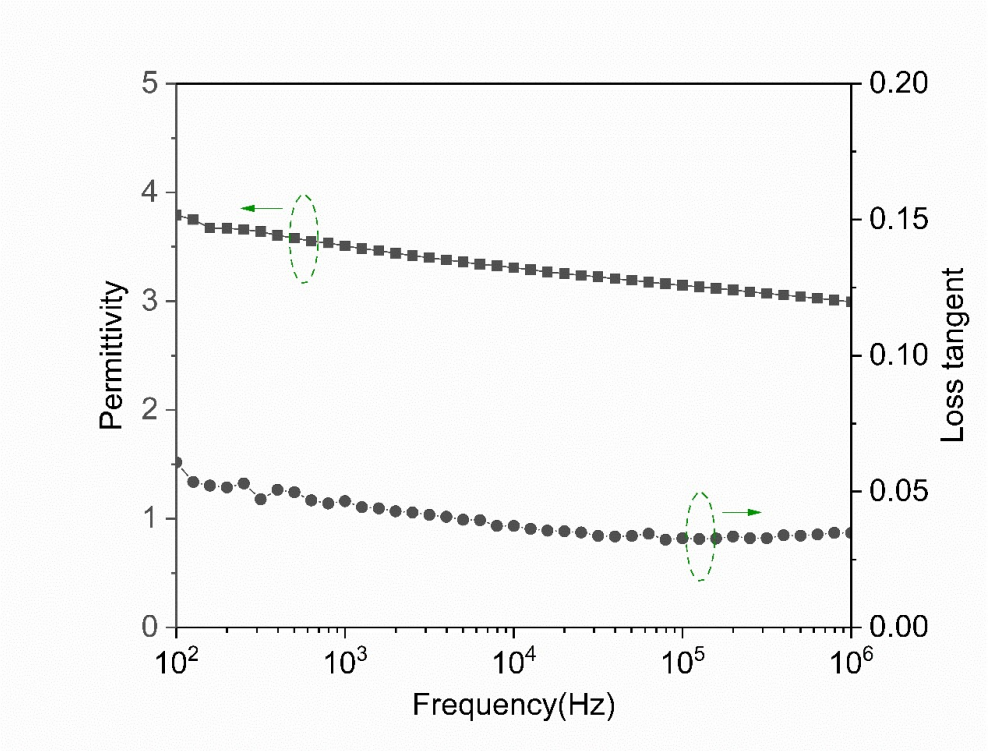

Fig. S5. Frequency dependence of the dielectric constant and dissipation factor of PMMA

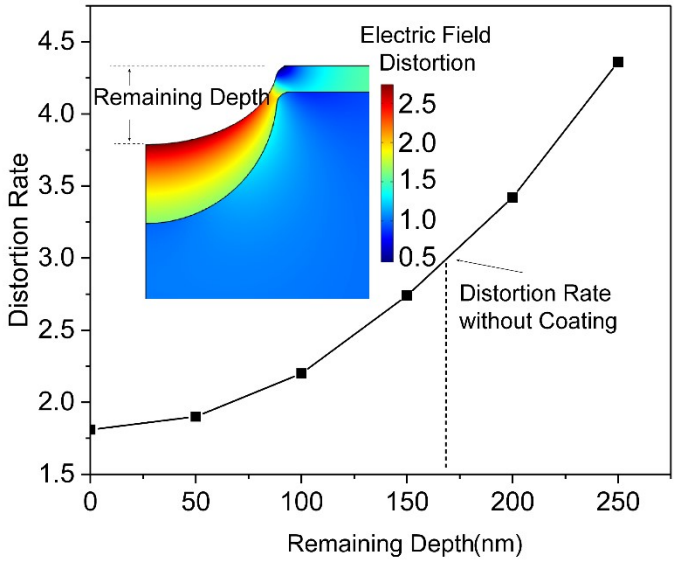

Fig. S6. Variation of distortion rate with the variation of remaining depth. The insets illustrate the electric field distortion near the electrode-dielectric interface.

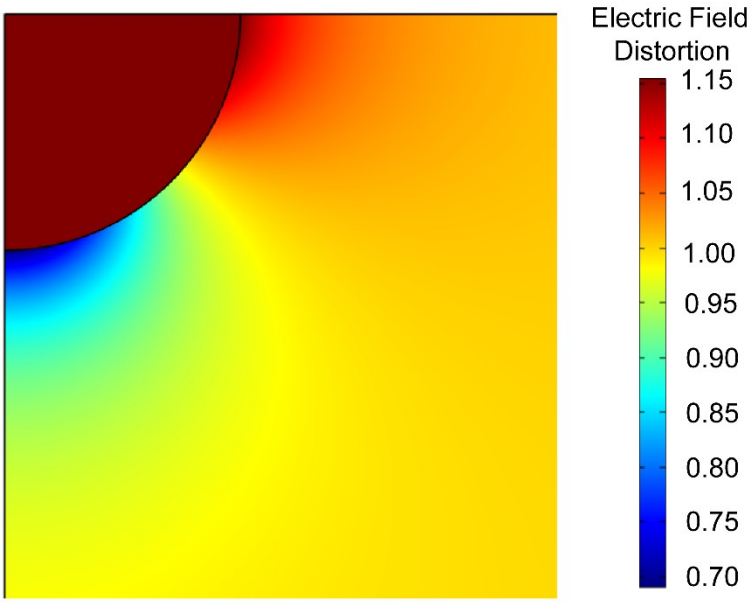

Fig. S7. The distribution of electric field strength with surface hole shape defect just fully filled.

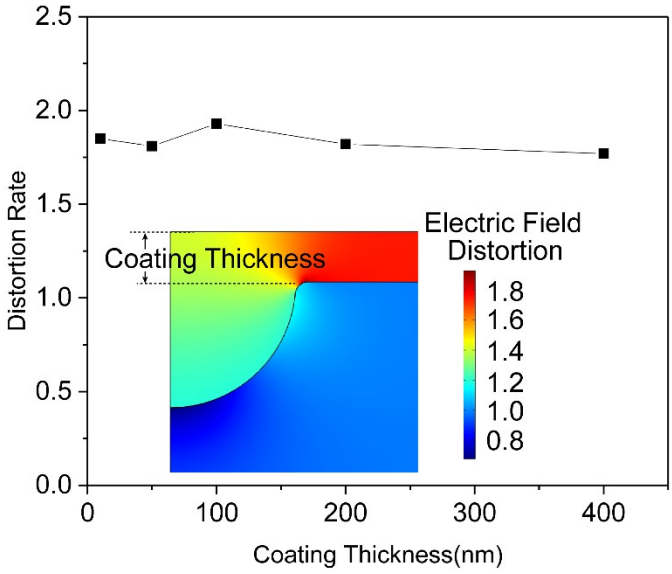

Fig. S8. Variation of distortion rate with the variation of coating thickness. The insets illustrate the electric field distortion near the electrode-dielectric interface.

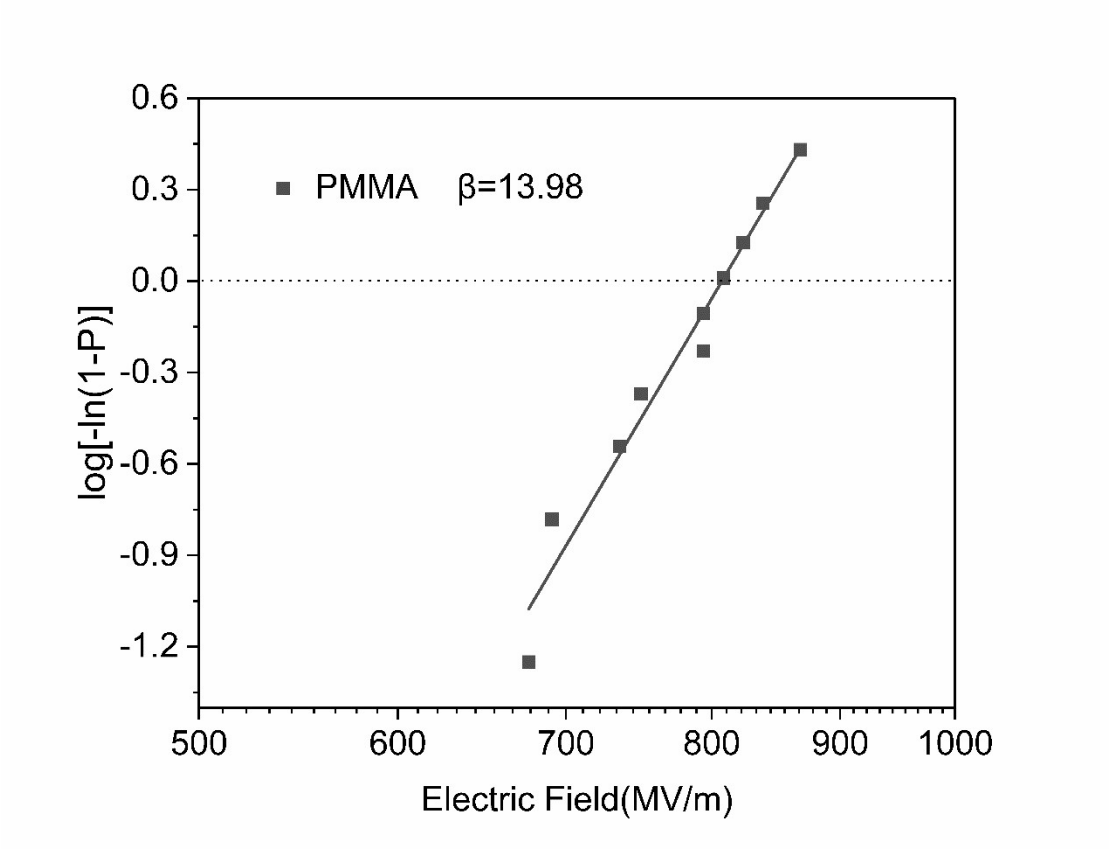

Fig. S9. Weibull distribution analysis of the breakdown strength of PMMA.

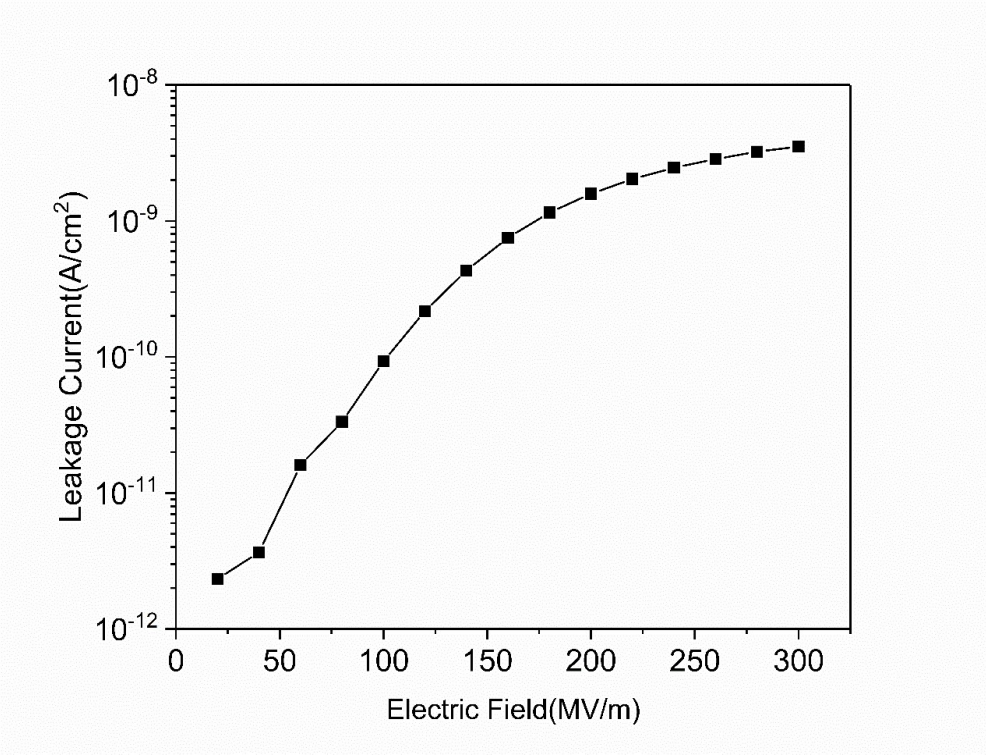

Fig. S10. Variation of PMMA leakage current with applied voltage, the thickness of PMMA sample is 6.8μm.

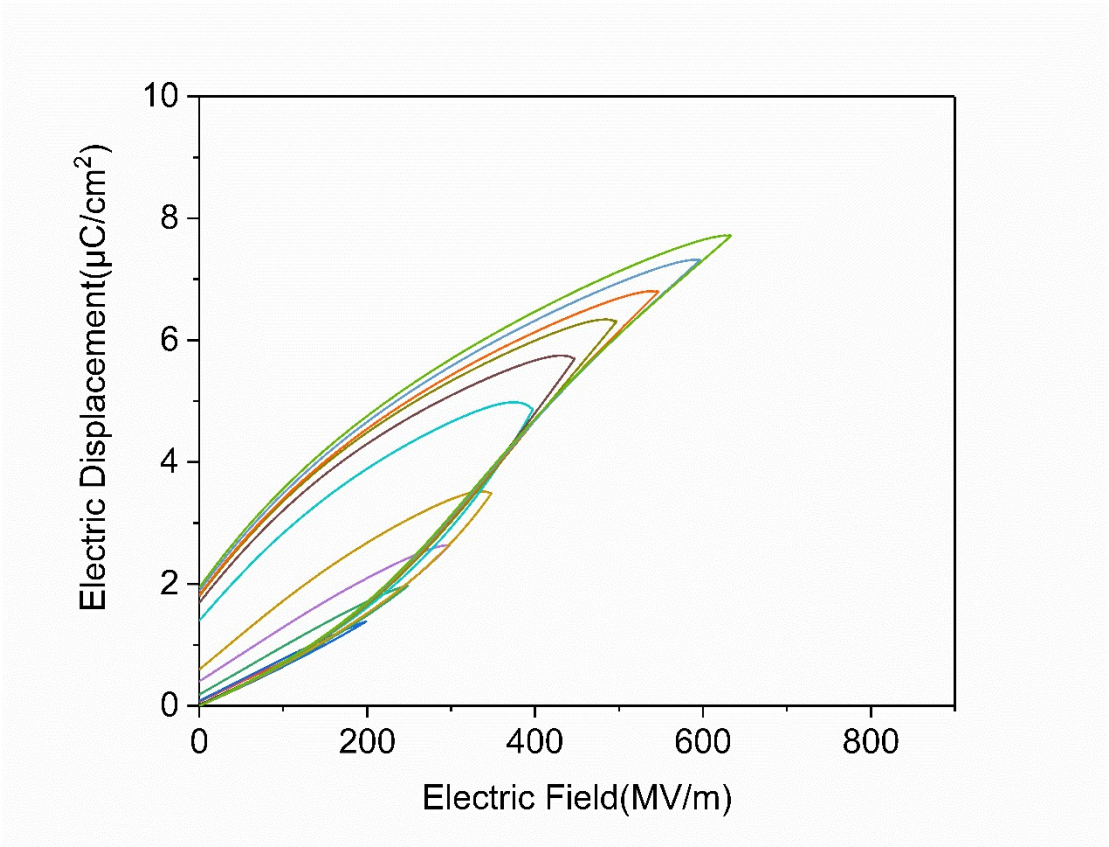

Fig. S11. Electric displacement–electric field loop of pure PVDF film.

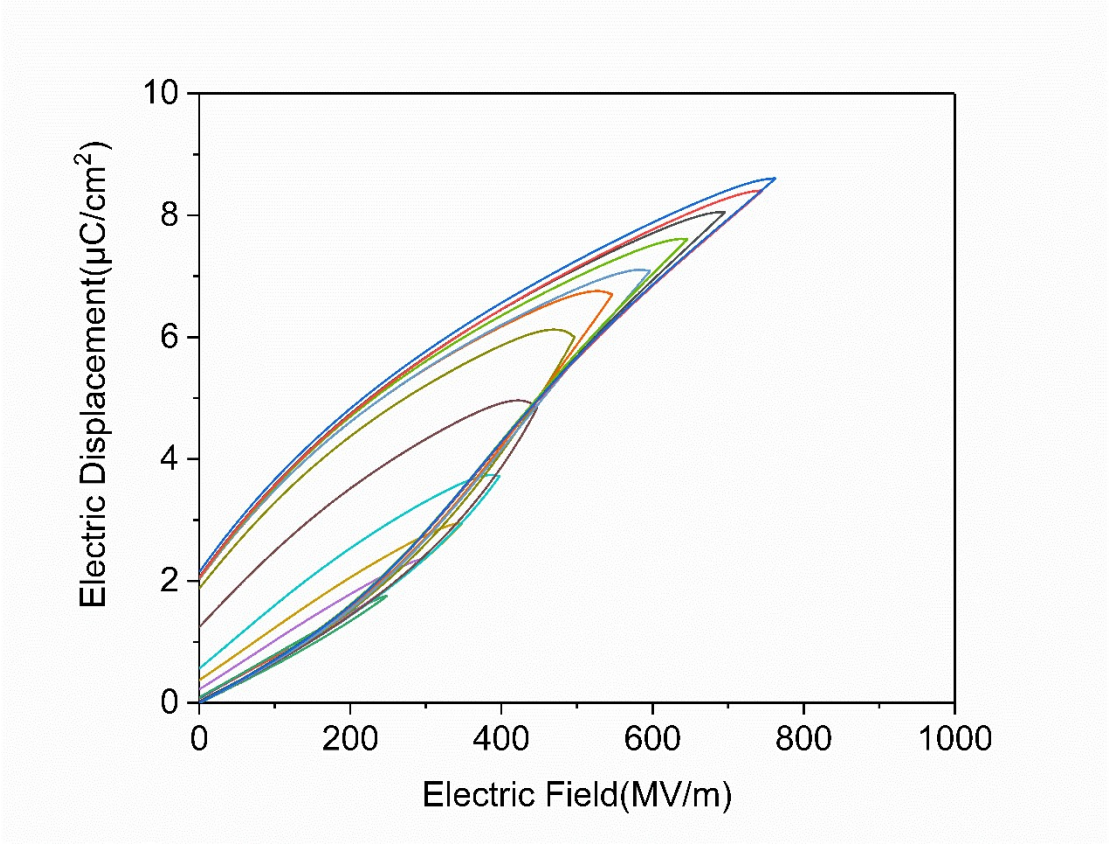

Fig. S12. Electric displacement–electric field loop of double-layer composite film

with 0.1%wt coating PMMA.

Calculation of time constant

$$\tau_{PVDF} = R * C_{PVDF} = 100 * 10^{3} * 8.85 * 10^{-12} * 6.69 * \frac{0.1256 * 10^{-4}}{9 * 10^{-6}} \approx 8.26\ \mu s$$

$$\tau_{BOPP} = R * C_{PVDF} = 100 * 10^{3} * 8.85 * 10^{-12} * 2.2 * \frac{0.1256 * 10^{-4}}{4.88 * 10^{-6}} \approx 5.01\ \mu s$$

$$\frac{\tau_{PVDF}}{\tau_{BOPP}} \approx 1.65$$

The discharge time of PVDF(t_{PVDF}) is 22.1μs and the discharge time of BOPP(t_{BOPP}) is 14.4μs.

$$\frac{t_{PVDF}}{t_{BOPP}} \approx 1.53$$

The difference of results mainly comes from the resistance of film capacitor and the permittivity measured at low field and fixed frequency.